World Electric Vehicle Journal

Article

Design and Implementation of a Wireless Power Transfer System for Electric Vehicles

Vekil Sari

Department of Electrical & Electronics Engineering, Sivas Cumhuriyet University, Sivas 58140, Turkey; vsari@cumhuriyet.edu.tr

Abstract: Wireless power transfer (WPT) systems, which have been around for decades, have recently become very popular with the widespread use of electric vehicles (EVs). In this study, an inductive coupling WPT system with a series–series compensation topology was designed and implemented for use in EVs. Initially, a 3D Maxwell (ANSYS Electromagnetics Suite 18) model of the system was generated. The impact of individual parameters on the coupling coefficient was analyzed through systematic variations in each parameter's values. As a result, a system with a higher coupling coefficient was obtained. Using this system, three distinct load cases were investigated for their efficiency in the Simplorer (ANSYS Electromagnetics Suite 18) circuit. Subsequently, a prototype of the system was constructed, and the experimental results were compared with the model's results. This study shows that both the output power and the efficiency of the system increase as the load resistance increases. The results obtained in this study are anticipated to offer valuable insights for the enhancement of WPT system design.

Keywords: wireless power transfer; inductive wireless power transfer; series–series compensation

Citation: Sari, V. Design and Implementation of a Wireless Power Transfer System for Electric Vehicles. *World Electr. Veh. J.* **2024**, *15*, 110. https://doi.org/10.3390/wevj15030110

Academic Editors: Zhizhen Liu and Yanjin Hou

Received: 23 January 2024
Revised: 5 March 2024
Accepted: 9 March 2024
Published: 12 March 2024

1. Introduction

The uncontrolled use of natural resources such as oil leads to a decrease in these re-sources, and humanity will face a shortage of natural energy resources in the future. Electricity is an alternative source that can replace gasoline in vehicles. Additionally, EVs do not cause environmental pollution due to having zero greenhouse gas emissions [1].

Electrical power can be transmitted to devices through two primary methods: wired and wireless. Wired power transfer is acceptable in some environments but may be unsafe or may have a limited lifetime in humid environments [2]. The concept of WPT was demonstrated by Nikola Tesla in 1891 [3]. WPT is advantageous in that it is simple, weather-proof, spark-free, robust, and reliable [4,5]. Owing to these advantages, applications of WPT have progressively expanded over time and it has emerged as a pivotal technology [6]. Today, WPT is used in many fields, such as industry, biomedicine, cleaning, consumer electronics, and EVs [7,8]. The transmitted power level varies from a few milliwatts to tens of kilowatts [9].

WPT systems for EVs can be divided into two main groups: short-air-gap WPT systems and long-air-gap WPT systems. Short-air-gap WPT systems include coupled magnetic resonance, inductive WPT, and capacitive WPT [10]. In inductive WPT, a frequency lower than 200 KHz is used, and the coupling coefficient is greater than 0.1 [11].

In WPT for EVs, the separation distance between the transmitter and the receiver typically ranges from 10 to 40 cm [12], while an electrical current within the range of 3 to 400 A can be employed [13]. The charging methods for EVs can be categorized into three levels. Level 1 charging is feasible at home or office environments utilizing a single-phase AC system, with charging durations ranging between 4 and 36 h. Level 2 charging, available in private or public locations, employs either a single-phase or three-phase AC system, with charging durations spanning from 1 to 6 h. Level 3 charging, facilitated at gas stations and commercial establishments, employs a DC or three-phase AC system, with charging times typically ranging from 0.2 to 1 h [14]. Numerous car manufacturers are actively integrating WPT systems into their EVs [15]. As a result of the increase in the transfer power and efficiency of WPT systems for EVs, it is likely that wireless charging will replace traditional conductive charging in the foreseeable future [16]. Wireless charging in EVs can be classified into two operational modes: static and dynamic. In static WPT, the vehicle remains stationary throughout the charging process, whereas in dynamic wireless charging, the vehicle is charged while in motion [17].

WPT systems consist of transmitters and receivers. The transmitter consists of a DC power supply, semiconductor switches switching at a high frequency, a capacitor for compensation, and a transmitter coil. The receiver consists of the receiver coil, a capacitor for compensation, a rectifier circuit, and the load. In WPT systems, there may be only one transmitter and one receiver, or there may be multiple transmitters [18] and receivers [19]. Figure 1 shows a WPT system consisting of a transmitter and a receiver. Ferrite bars can be utilized to help direct and shape the flux path in WPT systems [20].

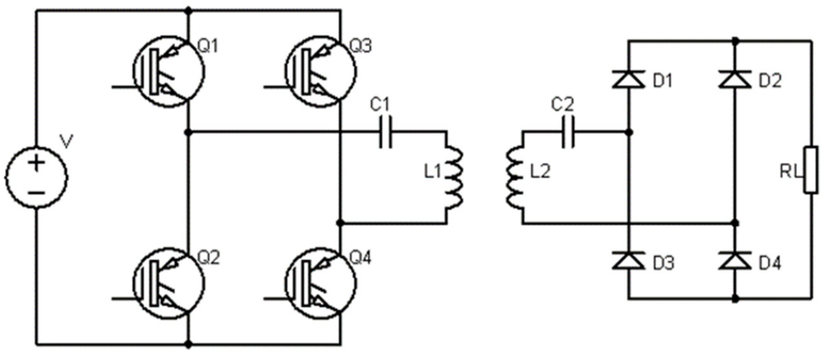

Figure 1. General circuit diagram of the WPT system.

The interference caused by the intrusion of metal objects between the transmitting and receiving coils adversely affects the system's performance. Previous research indicates that the system's efficiency diminishes in the presence of aluminum, copper, and iron objects positioned between the transmitter and receiver coils [21]. Furthermore, studies have demonstrated that non-ferromagnetic metal objects experience a pushing force, whereas ferromagnetic objects undergo a pulling force when placed between the coils [22]. Implementing a metal object detection system within the WPT system can mitigate these challenges.

In WPT research, optimizing system performance in terms of both time and cost necessitates the preliminary generation and analysis of system models using simulation programs before the practical implementation of the system. Previous studies have employed various simulation software packages, including Ansys Maxwell [9,23–25], JMAG [26,27], and COMSOL [28], to develop and evaluate 3D models of WPT systems.

WPT systems utilize various coil shapes, including circular, square, rectangular, circular-rectangular, double D (DD), double D quadrature (DDQ), and bipolar polarized (BP) designs [29]. While spiral circular coils offer an enhanced coupling efficiency, square and rectangular coils demonstrate a superior level of tolerance to misalignment [30].

Figure 2 illustrates the dimensions of the circular coil used for a mutual inductance calculation. The mutual inductance of the circular coil can be computed using Equations (1) and (2) [31]. Lateral misalignment changes the mutual inductance, significantly impacting the system's coupling coefficient and efficiency.

$$M = \mu_0 N_1 N_2 \pi \sqrt{R_a R_b} \left(\frac{F_k^3}{16} + 3\frac{F_k^3}{64} \right) \tag{1}$$

$$F_k = \sqrt{\frac{4 R_a R_b}{(R_a + R_b)^2 + h^2}} \tag{2}$$

Here, M is the mutual inductance, μ_0 is the vacuum permeability, N_1 is the number of turns of the receiver coil, N_2 is the number of turns of the transmitter coil, R_a is the radius of the inner turn of the receiver coil, R_b is the radius of the inner turn of the transmitter coil, and h is the distance between the coils.

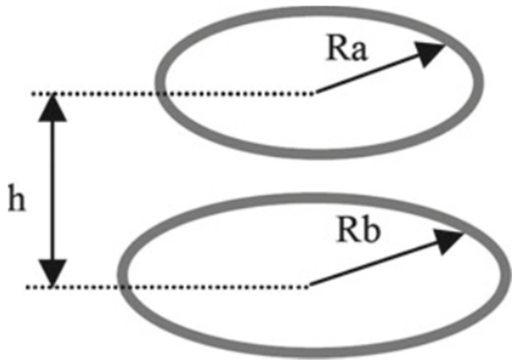

Figure 2. Circular coil's dimensions for calculating M.

Since coils are used in inductive coupling WPT systems, the system inherently becomes inductive. The inductance increases with the frequency of the source, contributing to a low power factor and increased losses. Compensation becomes necessary to enhance the power factor, requiring the connection of capacitors to both the transmitter and receiver sides. The transferred power can be amplified up to 50 times by compensation [32]. To understand the significance of compensation, the uncompensated equivalent of the system must be considered. In Figure 3, the transmitter and receiver coils are shown as a winding and a resistor. The system can be described with Equations (3) and (4) [31].

$$V_1 = (R_1 + jwL_1)I_1 - jwMI_2 \tag{3}$$

$$jwMI_1 = (R_2 + jwL_2 + R_L)I_2 \tag{4}$$

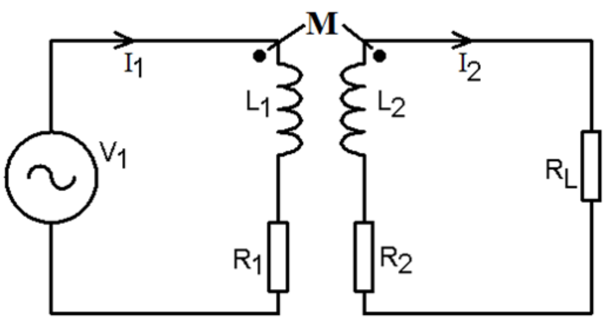

Figure 3. Equivalent circuit of inductive coupling WPT.

By employing Equations (3) and (4), the current ratio is computed as shown in Equation (5). The efficiency of the system is derived using Equation (6). Equation (7) is obtained by substituting the current ratio from Equation (5) into Equation (6) [31].

$$\frac{I_1}{I_2} = \frac{jwL_2 + R_2 + R_L}{jwM} \tag{5}$$

$$\eta = \frac{R_L I_2^2}{R_L I_2^2 + R_2 I_2^2 + R_1 I_1^2} = \frac{R_L}{R_L + R_2 + R_1\left(\frac{I_1}{I_2}\right)^2} \tag{6}$$

$$\eta = \frac{R_L}{R_L + R_2 + R_1\frac{(R_2+R_L)^2+(wL_2)^2}{w^2M^2}} \tag{7}$$

When the system is not compensated, it is evident that the self-inductance L_2 appears in the denominator of Equation (7) [31]. Since this term is always positive, it leads to a decrease in efficiency. Compensating the system allows for the elimination of this term, consequently resulting in an increase in efficiency.

Four fundamental compensation topologies are established based on whether the capacitors are connected to the coil in series or parallel: SS, SP, PS, and PP. The letters S and P denote the serial and parallel connection of the capacitor to the coil, respectively. Figure 4 illustrates these compensation topologies [33]. Each of these four topologies possesses distinct advantages and disadvantages, and the choice generally depends on the type of application. However, for general WPT systems, the SS topology is more advantageous than the others [34,35]. One advantage of series compensation is the absence of reflected reactance at the secondary resonance frequency. On the other hand, parallel compensation reflects capacitive reactance at the resonance frequency [36]. In addition to these four basic topologies, studies have also explored the SPS topology, which integrates aspects of both the SS and SP topologies. As a result of a previous study, it was concluded that the misalignment tolerance of the SPS topology surpasses that of others [37].

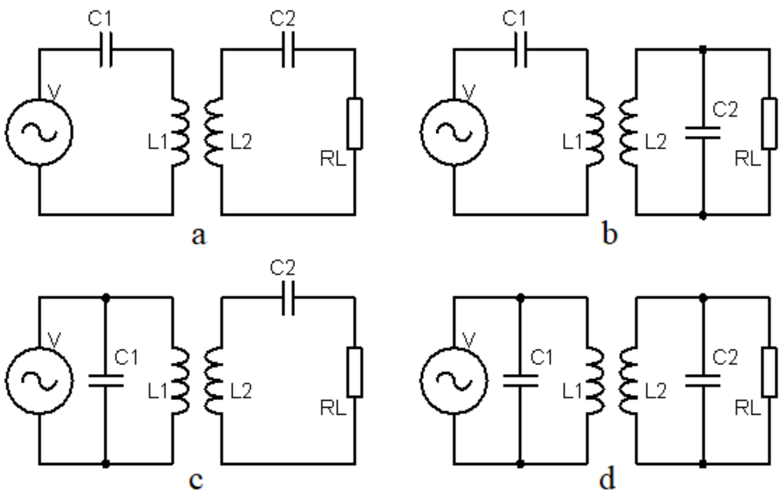

Figure 4. Compensation topologies: (**a**) SS, (**b**) SP, (**c**) PS, and (**d**) PP.

In series–series compensation, the values of the transmitter and receiver capacitors can be computed using Equations (8) and (9) [26]. Additionally, the quality coefficients of the transmitter and receiver coils can be calculated with Equations (10) and (11) [38].

$$C_1 = \frac{L_2 C_2}{L_1} \tag{8}$$

$$C_2 = \frac{1}{w^2 L_2} \tag{9}$$

$$Q_1 = \frac{R_L L_1}{w M^2} \tag{10}$$

$$Q_2 = \frac{w L_2}{R_L} \tag{11}$$

Here, L_1 is the primary coil inductance, L_2 is the secondary coil inductance, M is the mutual inductance, C_1 is the primary capacitor, C_2 is the secondary capacitor, ω is the resonant frequency, and R_L is the load resistance.

Equation (12) illustrates the relationship between the coupling coefficient and mutual inductance [36]. In WPT systems, the power transfer depends on the coupling coefficient, which, in turn, depends on the coil design [39]. Moreover, the coupling coefficient also depends on the precise alignment of the coils. Misalignment between the transmitter and receiver coils may reduce the coupling coefficient and the efficiency of the system. The power transferred to the receiver coil can be determined using Equation (13) [1].

$$k = \frac{M}{\sqrt{L_1 L_2}} \tag{12}$$

$$P = \frac{w^2 M^2 I_1^2}{R_L} \tag{13}$$

Here, I_1 is the current flowing through the transmitter coil.

Numerous studies have explored inductive coupling WPT systems. Some of these studies are given in Table 1. Upon examination of the studies presented in Table 1, it is evident that power levels range from 9 to 6600 W. The prevailing compensation topology is SS, with distances varying between 3 and 30 cm, frequencies ranging from 18.65 to 105 KHz, and efficiencies spanning from 79.48% to 98%.

Table 1. Previous inductive coupling WPT studies.

Ref.	Power (W)	Compensation Topology	Distance (cm)	Frequency (KHz)	Efficiency (%)	Year
[4]	5000	LCL	17.5–26.5	20	90	2012
[7]	3000	SS	10	35	95.8	2015
[8]	9	SS	3	43.2	80–92	2023
[9]	3000	LCC	15	85	95.5	2017
[11]	3000	SP	12–20	50	90	2012
[12]	4000	SS	4	80	97	2014
[18]	34	SS	N/A	100	91	2017
[19]	1500	LCL	4	20	85	2011
[34]	100	SS	5	105	83.2	2011
[35]	2180	SS	12.5	18.65	90	2015
[37]	2014	SPS	15	19.6	92	2011
[39]	3700	SS	12	85	90.02	2023
[40]	1200	SS	4	83.3	98	2022
[41]	500	SS	10–15	85	80	2022
[42]	266.9	SS	10	85	79.48	2021
[43]	500	LCC	N/A	85	95	2020
[44]	3000	LCL	30	85	95	2020
			12.5		97.6	
[45]	6600	SS	21	86.5	95.5	2024
			25		93.1	

In this study, an inductive WPT system was designed and prototyped. Initially, the Maxwell model of the system was generated, focusing on increasing the coupling coefficient. Four parameters were identified, and their impact on the coupling coefficient was investigated. One of the critical parameters of the inductive WPT system is the coupling coefficient. The efficiency of the system increases with the coupling coefficient. This study is significant as it shows how these parameters affect the coupling coefficient. In contrast to the previous study, which reported a coupling coefficient of 0.1625 and an efficiency of 78.3, the current study achieved a higher coupling coefficient of 0.2671 and an efficiency of 81.4 by optimizing the four parameters. The proper selection of system parameters can substantially enhance system efficiency. While the efficiency in this study appears to be slightly low, future research can explore parameters aimed at further increasing this. Potential investigations may include examining the impact of the coil shape, operating frequency, and compensation topology on the system efficiency.

1.1. Life Cycle Assessment of WPT Systems

A life cycle assessment (LCA) is necessary to evaluate the environmental impacts of WPT systems. An LCA assesses the entire life cycle of a product adopting a "cradle-to-grave" approach to evaluating industrial systems. The "cradle-to-grave" concept begins with the extraction of raw materials from the earth to create the product and concludes when all materials are returned to the environment. An LCA offers a comprehensive view and precise evaluation of the environmental aspects of a product or process throughout the product's life cycle. The term "life cycle" refers to the key activities that occur throughout the life of the product, spanning from its production and its use and maintenance, including the acquisition of raw materials essential for production, to its final disposal. Figure 5 illustrates the potential life cycle stages considered in an LCA along with the inputs/outputs typically measured [46].

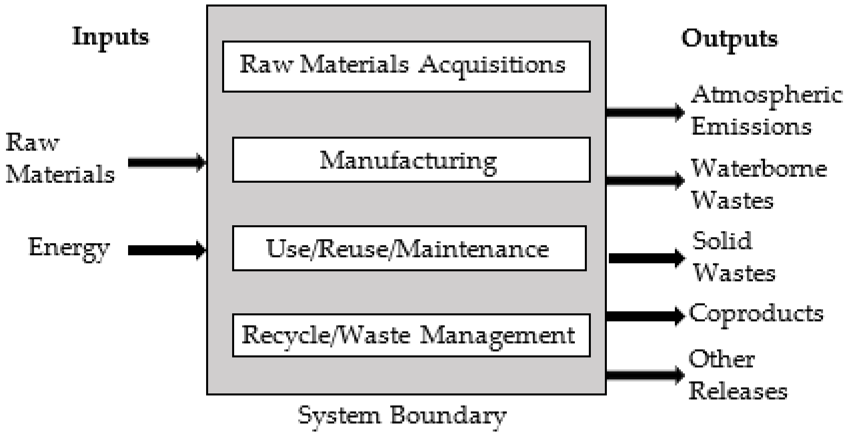

Figure 5. Life cycle stages.

To conduct an LCA of WPT systems, their advantages and disadvantages must be weighed comprehensively. In a previous study, a life cycle assessment of a WPT system was conducted, focusing on electric buses operating on a certain route within urban areas. WPT systems can be deployed at bus stations to charge electric buses used for urban passenger transportation. By charging the bus battery during pick-up and drop-off at each station, the battery size of the bus can be reduced. The charging infrastructure provided by dynamic WPT extends the range of EVs, allowing them to have a minimal battery size, and eliminating EV users' range anxiety.

However, WPT systems present both advantages and challenges. Charging while waiting or driving requires WPT infrastructure on the roads. This large-scale infrastructure will impose significant additional energy, environmental, and economic burdens. Moreover, challenges include the recognition of fast-moving WPT-EVs approaching charging lanes and the real-time computation of electricity costs billed to EV drivers. Other technical problems include equipment compatibility, electromagnetic shielding, and the detection and elimination of foreign objects in WPT systems.

Although the study suggests that the WPT system has a lower overall life cycle cost (LCC) compared to that of the plug-in charging system, there is a significant amount of uncertainty in this conclusion. The difference in LCC between plug-in charging and WPT largely depends on factors such as the battery unit price, WPT efficiency, and the costs associated with the purchase, installation, and maintenance of WPT infrastructure [47].

1.2. Safety of WPT Systems and Related Standards

The safety and performance of WPT systems can be increased by precautions taken during their design, production, and use. These precautions are important to ensure the safety of both users and vehicles. The main issues and precautions that can be taken regarding the safety of WPT systems for EVs are as follows:

1. Electromagnetic compatibility (EMC): The WPT system must comply with electromagnetic compatibility requirements. This allows the device to operate in harmony with other electronic equipment and minimize electromagnetic interference [48].

2. Foreign object detection (FOD): Wireless chargers must be able to detect foreign objects under the vehicle being charged. This prevents the device from accidentally operating on a foreign object and increases safety [28].
3. Temperature control: Temperature sensors and control mechanisms should be used to reduce the risk of overheating during wireless charging [49].
4. User safety: Wireless chargers should have features that protect the user [50].
5. Compliance with standards: WPT systems must comply with relevant industry standards and regulations. This is important to ensure security and performance. The standards for WPT systems are as follows:
    - SAE J2954 is a standard for WPT for EVs led by Society of Automotive Engineers (SAE) International. SAE J2954 establishes a methodology for designing and testing WPT systems for EVs up to power levels of 11 kW. SAE J2954 includes the powering frequency, electrical parameters, specifications, procedures, and other factors to be evaluated. It describes the specific dimensions for ground assembly (GA) and vehicle assembly (VA) components, including the power transmitting coil and receiving coil, respectively [51].
    - IEC 61980-1 covers the general requirements for EV WPT systems including a general background and definitions (e.g., efficiency, electrical safety, EMC, and EMF). IEC 61980-2 specifically applies to magnetic field (MF) WPT for EVs and covers specific requirements for system activities and communication between the EV side and the off-board side including a general background and definitions. IEC 61980-3 covers specific power transfer requirements for the off-board side of MF-WPT for EVs (e.g., efficiency, electrical safety, EMC, and EMF) [52].
    - ISO 19363:2020 defines the requirements and operation of the on-board vehicle equipment that enables magnetic field (MF) WPT for charging the traction battery of EVs. It is intended to be used for passenger cars and light duty vehicles [53].

1.3. Scalability of WPT Systems and Their Potential for Future Development

The scalability of WPT systems for EVs refers to their ability to efficiently and effectively accommodate an increasing number of vehicles and charging stations in a growing market. The following are some of their key aspects, potential ways to enhance their scalability, and idea for future developments:

- Standardization and compatibility: The standardization of WPT systems ensures interoperability among different manufacturers and vehicle models. This promotes their wider adoption and scalability.
- Grid integration: Integrating WPT systems into the grid infrastructure allows for the deployment of charging points in various locations, such as parking lots, highways, and roadsides. This enhances scalability by providing more charging options.
- High efficiency and power levels: Improving the efficiency and power levels of WPT systems enables faster charging and the ability to charge multiple vehicles simultaneously, enhancing scalability.
- Cost and economic efficiency: Reducing the cost of WPT systems while improving economic efficiency can increase their adoption and scalability. Lower costs make the technology more accessible to a larger user base.
- Ubiquitous availability: Ensuring the widespread availability of wireless charging infrastructure increases scalability. This involves deploying charging points in a variety of locations to provide users with more convenient access.

The adaptability of WPT systems to different vehicle types and for future developments in WPT technology is an important issue. Future developments in WPT systems could include the following:

- Higher power levels: WPT systems capable of operating at higher power levels would allow for faster charging.
- Smart charging management: Implementing smart charging management systems can optimize energy usage, improve efficiency, and balance the load on the grid.

- Automation and remote management: Automation and remote management features can make charging processes easier and more efficient.
- Energy storage integration: The integration of energy storage systems, such as battery storage, with WPT systems can increase energy efficiency and balance energy flow.
- Improvements in environmental and economic factors: Using more environmentally friendly materials, improving manufacturing processes, and reducing costs can enable WPT systems to reach a wider user base.

1.4. Validation Process and Reliability Tests of WPT Systems

The validation process and reliability tests of WPT systems used in EVs are usually carried out based on international standards. These processes are important to ensure the safe, efficient, and compatible operation of WPT systems. This verification process and the reliability tests can be divided into five categories as follows:

1. Conformance and validation standards: The validation process of WPT systems is generally carried out in line with international standards, especially standards such as SAE J2954. These standards include various tests that determine the suitability and performance of WPT systems.
2. Electromagnetic compatibility (EMC) tests: EMC tests determine whether WPT systems are compatible with other devices in the electromagnetic spectrum. These tests are performed to ensure that electromagnetic radiation and interference are under control.
3. Efficiency and safety tests: The efficiency and safety of WPT systems are tested. While efficiency tests determine how efficiently the system transfers energy, safety tests ensure that the system operates without harming people and the environment.
4. Durability and environmental tests: WPT systems are subjected to various durability and environmental tests. These tests determine how the system performs in changing weather conditions and with long-term use.
5. Compatibility tests: Compatibility tests are performed to determine whether WPT systems are compatible with different vehicle models and manufacturers. These tests are important to verify that the system is suitable for a wide range of users.

The validation and reliability testing of WPT systems involves a combination of these and similar tests and is usually performed by manufacturers.

1.5. The User Experience and Integration Aspects of WPT Systems

The user experience and integration aspects of WPT systems used in EVs aim to enable users to perform the charging process easily, safely, and efficiently. These factors facilitate the process of charging users' EVs and contribute to the widespread adoption of WPT systems. We can divide these aspects into six categories as follows:

1. User-friendly design: WPT systems must have a user-friendly design. The location of charging points should be accessible and easy to use. Users should use minimal effort to start and stop charging.
2. Automatic detection and start: WPT systems must automatically start charging by detecting the vehicle's location. This allows users to charge their vehicles easily without any manual intervention.
3. Security and protections: WPT systems must have various security and protection measures to ensure the safety of users and vehicles. These may include features such as short circuit protection, overcurrent protection, and leakage protection.
4. Integration and smart charging management: WPT systems must have smart charging management features. These features can be used to improve energy efficiency, balance the load on the grid, and optimize users' charging processes.
5. Environmental awareness: WPT systems must demonstrate environmental sensitivity. This includes factors such as energy efficiency, the use of recycled materials, and waste management.
6. Ease of integration: WPT systems should be easily integrated with EVs and grid infrastructure. This makes it easier for users to expand or improve charging infrastructure.

2. Materials and Methods

This paper aims to increase the coupling coefficient (*k*) of the system detailed in a previous study [54] by changing some parameters. Increasing the coupling coefficient of the system inherently enhances its efficiency. Parameters under examination included the following: coating the outer surface of the coils with ferrite, altering the number of windings of the coils, adjusting the inner and outer radii of the transmitter and receiver coils, and modifying the step distance between the windings.

The flow chart of the implemented inductive WPT system methodology is presented in Figure 6. The initial step involves determining the design parameters. This includes defining the characteristics of the battery to be charged (voltage, power, and resistance). Subsequently, the selection of the voltage source and switching elements for charging the battery, determination of the number of windings for the transmitter and receiver coils, and specification of the conductor cross-sections are established. The second step entails determining the compensation topology with the SS topology selected in this study. The next step is to generate the Maxwell model of the system. Parameters to be examined, which total four in this study, are then identified. The subsequent step involves altering the first parameter and determining the corresponding *k* value for each parameter value. This process is repeated for all four parameters. Following an examination of these parameters, the parameters yielding the highest *k* values are determined, and a system prototype is constructed using these optimized parameters.

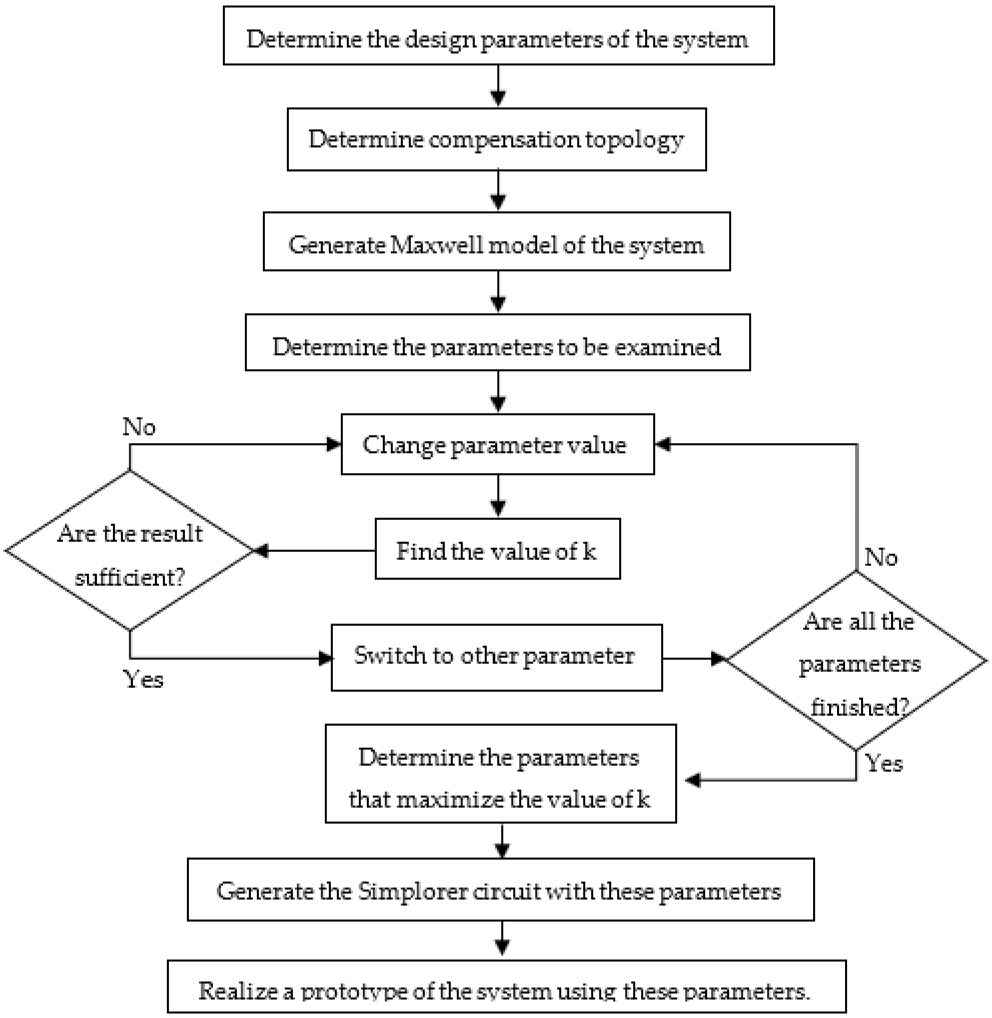

Figure 6. Methodology flow chart of WPT system.

The parameters of the previous study are shown in Table 2. Figure 7 shows the dimensions of the system.

Table 2. Parameters of previous work.

a	Distance between coils	200 mm
Tft	Transmitter ferrite thickness	0 mm
Rft	Receiver ferrite thickness	0 mm
N_1	Number of turns of the transmitter coil	20 turns
N_2	Number of turns of the receiver coil	20 turns
$Rtin$	Transmitter coil inner radius	100 mm
$Rrin$	Receiver coil inner radius	100 mm
$Rtout$	Transmitter coil outer radius	250 mm
$Rrout$	Receiver coil outer radius	250 mm
dt	Pitch length of transmitter coil	7.5 mm
dr	Pitch length of receiver coil	7.5 mm
k	Coupling coefficient	0.1625
L_1	Inductance of transmitter coil	161.95 µH
L_2	Inductance of receiver coil	155.74 µH
M	Mutual inductance	25.66 µH
C_1	Transmitter capacitor	391.41 nF
C_2	Receiver capacitor	407.12 nF
Q_1	Transmitter quality factor	9.791
Q_2	Receiver quality factor	3.911
f_0	Resonant frequency	20 KHz
V_{source}	Input voltage (RMS)	100 V
I_{source}	Input current (RMS)	40.4 A
P_{in}	Input power	4040 W
V_L	Load voltage (RMS)	125.79 V
I_L	Load current (RMS)	25.15 A
P_L	Output power	3163 W
R_L	Load	5 Ω
η	Efficiency	78.3

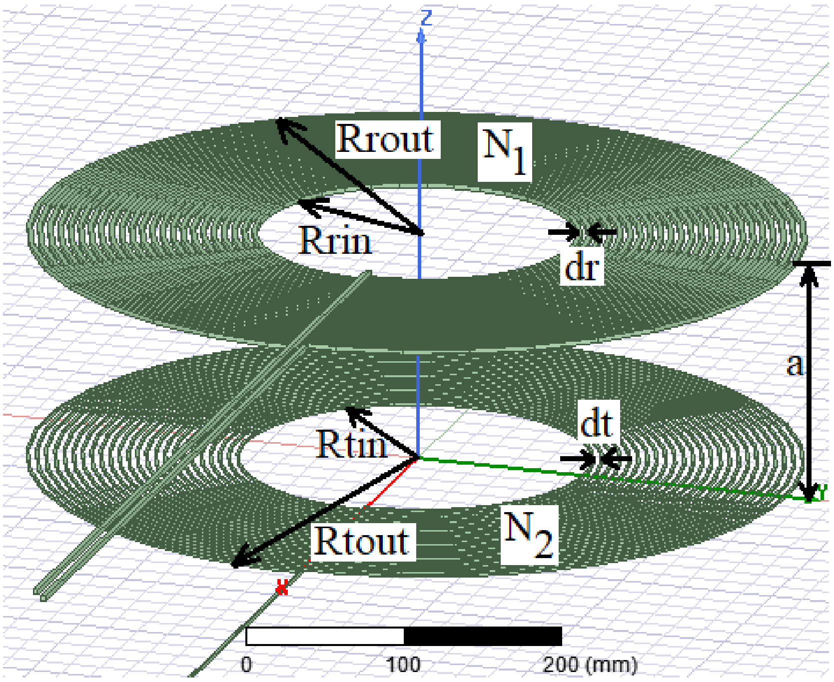

Figure 7. Dimensions of the inductive coupling WPT system.

2.1. Effect of Coating Coils with Ferrite on Coupling Coefficient

Initially, the effect of ferrite coating on the outer surfaces of the transmitter and receiver coils was investigated. Table 3 illustrates the coupling coefficient (k) values corresponding to different ferrite thicknesses. For these calculations, other parameters were held constant (N_1 = 20 turns, N_2 = 20 turns, dt = 7.5 mm, dr = 7.5 mm, $Rtin$ = 100 mm, $Rrin$ = 100 mm, $Rtout$ = 250 mm, and $Rrout$ = 250 mm).

Table 3. k values obtained according to ferrite thickness.

k		*Rft* (mm)					
		0	**1**	**2**	**3**	**4**	**5**
Tft (mm)	0	0.1625	0.1819	0.1831	0.1842	0.1847	0.1851
	1	0.1832	0.2074	0.2094	0.2102	0.2108	0.2112
	2	0.1847	0.2095	0.2109	0.2123	0.2129	0.2133
	3	0.1855	0.2104	0.2123	0.2132	0.2138	0.2143
	4	0.1860	0.2110	0.2130	0.2139	0.2145	0.2149
	5	0.1864	0.2115	0.2135	0.2144	0.2149	0.2154

As depicted in Table 3, when the ferrite thickness applied to the transmitter and receiver coils is 1 mm, the k value increases significantly. However, further increments in ferrite thickness do not lead to proportional increases in the k value. Since the receiver coil will be installed in the EV, it should be lightweight; a ferrite thickness (*Rft*) of 1 mm is deemed appropriate. Conversely, since the transmitter coil remains stationary, its weight is less critical; nevertheless, for cost effectiveness, a ferrite thickness (*Tft*) of 3 mm is suggested. In this scenario, the corresponding k value is 0.2104, reflecting a 29.47% increase in k.

2.2. Effect of Change in Number of Coil Windings on Coupling Coefficient

As a second parameter, the variation in k value according to the changes in the number of transmitter windings (N_1) and the number of receiver windings (N_2) was investigated.

Other parameters (Tft = 0 mm, Rft = 0 mm, dt = 7.5 mm, dr = 7.5 mm, $Rtin$ = 100 mm, $Rrin$ = 100 mm, $Rtout$ = 250 mm, and $Rrout$ = 250 mm) were held constant. The results are presented in Table 4.

Table 4. k values obtained according to the number of coil windings.

k		N_2								
		12	**13**	**14**	**15**	**16**	**17**	**18**	**19**	**20**
N_1	12	0.1048	0.1081	0.1115	0.1147	0.1176	0.1205	0.1227	0.1251	0.1273
	13	0.1085	0.1120	0.1156	0.1189	0.1221	0.1248	0.1274	0.1301	0.1325
	14	0.1120	0.1156	0.1194	0.1230	0.1263	0.1295	0.1321	0.1349	0.1374
	15	0.1152	0.1194	0.1233	0.1268	0.1303	0.1337	0.1365	0.1395	0.1422
	16	0.1183	0.1224	0.1265	0.1304	0.1341	0.1374	0.1407	0.1438	0.1466
	17	0.1212	0.1254	0.1297	0.1339	0.1378	0.1414	0.1449	0.1480	0.1510
	18	0.1239	0.1285	0.1328	0.1371	0.1412	0.1450	0.1484	0.1520	0.1552
	19	0.1264	0.1312	0.1356	0.1401	0.1444	0.1484	0.1520	0.1556	0.1592
	20	0.1287	0.1336	0.1383	0.1429	0.1473	0.1516	0.1553	0.1592	0.1625
	21	0.1308	0.1359	0.1407	0.1455	0.1502	0.1545	0.1585	0.1625	0.1663
	22	0.1327	0.1381	0.1430	0.1480	0.1528	0.1573	0.1615	0.1656	0.1696
	23	0.1346	0.1400	0.1453	0.1502	0.1552	0.1599	0.1644	0.1685	0.1727
	24	0.1362	0.1418	0.1470	0.1523	0.1574	0.1623	0.1670	0.1713	0.1755
	25	0.1377	0.1434	0.1488	0.1542	0.1594	0.1645	0.1693	0.1740	0.1782
	26	0.1390	0.1449	0.1506	0.1559	0.1613	0.1665	0.1715	0.1763	0.1806

Given that the receiver component must remain lightweight, it is suggested to choose N_2 = 20 windings. Conversely, since the transmitter component remains stationary, a higher k value can be achieved by increasing the number of windings. Consequently, N_1 = 26 windings was selected. The corresponding k value is 0.1806, representing an 11.13% increase in the k value.

2.3. Effect of Coil Inner and Outer Radius Changes on Coupling Coefficient

The inner and outer radii of the coils were considered as the third parameter. The impact of altering the inner and outer radii of the coils ($Rtin$, $Rtout$, $Rrin$, $Rrout$) on the coupling coefficient was examined while the other parameters remain unchanged (Tft = 0 mm, Rft = 0 mm, N_1 = 20 turns, N_2 = 20 turns, dt = 7.5 mm, and dr = 7.5 mm).

Our analysis from Table 5 indicates that when the inner radius increases (dt and dr are constant), the outer radius also increases. Notably, the k value increases as the inner radius increases, with a corresponding increase in the outer radius. However, it increases in the areas covered by the coils.

Given that the receiver coil will be situated within the EV, its weight should be minimized, and its size should be compact. Hence, it is recommended to set the outer radius of the transmitter coil to 320 mm, the inner radius to 170 mm, the outer radius of the receiver coil to 280 mm, and the inner radius to 130 mm. In this configuration, the corresponding k value is 0.2012, representing a 23.81% increase. The outer radii of the transmitter and receiver coils were calculated with Equations (14) and (15).

$$Rtout = Rtin + N_1.dt \tag{14}$$

$$Rrout = Rrin + N_2.dr \tag{15}$$

Table 5. Change in k value according to the inner and outer radii of the coils (dt and dr are constant).

K		***Rrin* (mm) *Rrout* (mm)**						
		70 220	**80 230**	**90 240**	**100 250**	**110 260**	**120 270**	**130 280**
Rtin (mm) *Rtout* (mm)	80 230	0.1382	0.1434	0.1481	0.1522	0.1557	0.1585	0.1607
	90 240	0.1425	0.1482	0.1533	0.1578	0.1617	0.1650	0.1676
	100 250	0.1462	0.1523	0.1579	0.1625	0.1672	0.1709	0.1740
	110 260	0.1493	0.1558	0.1618	0.1672	0.1721	0.1763	0.1798
	120 270	0.1521	0.1587	0.1652	0.1710	0.1764	0.1810	0.1850
	130 280	0.1540	0.1613	0.1679	0.1742	0.1800	0.1851	0.1896
	140 290	0.1553	0.1630	0.1700	0.1767	0.1829	0.1885	0.1935
	150 300	0.1561	0.1641	0.1717	0.1788	0.1852	0.1913	0.1967
	160 310	0.1565	0.1647	0.1726	0.1801	0.1869	0.1936	0.1993
	170 320	0.1563	0.1647	0.1729	0.1808	0.1882	0.1949	0.2012

2.4. Effect of Change in Distance between Coil Windings on Coupling Coefficient

As the final parameter, the distances between turns of the transmitter winding (dt) and the receiver winding (dr) were investigated considering their impact on the coupling coefficient k. Other parameters remained constant (Tft = 0 mm, Rft = 0 mm, N_1 = 20, N_2 = 20, $Rtout$ = 250 mm, and $Rrout$ = 250 mm).

While the outer radius remains constant, changes in the distances between windings result in alterations to the inner radius. The highest k value was obtained when dt = 7 mm and dr = 7 mm, yielding k = 0.1632. Consequently, the k value increased by 0.4%. These results are presented in Table 6.

Table 6. Change in k value according to the distance between coil windings.

k		***dr***					
		6	**6.5**	**7**	**7.5**	**8**	**8.5**
dt	6	0.1627	0.1629	0.1628	0.1629	0.1625	0.1620
	6.5	0.1628	0.1630	0.1630	0.1631	0.1627	0.1623
	7	0.1625	0.1629	0.1632	0.1630	0.1627	0.1625
	7.5	0.1622	0.1628	0.1629	0.1625	0.1625	0.1623
	8	0.1616	0.1624	0.1625	0.1624	0.1621	0.1620
	8.5	0.1613	0.1618	0.1619	0.1618	0.1616	0.1615

2.5. System with Increased Coupling Coefficient

Following the investigations, a system with a higher coupling coefficient was achieved and the Maxwell model of this system was generated. Figure 8 illustrates the magnetic field representation of the Maxwell model. The system parameters are presented in Table 7. Capacitor values C_1 and C_2 in Table 7 were determined using Equations (8) and (9). Subsequently, using these values, the Simplorer circuit of the system was constructed as depicted in Figure 9.

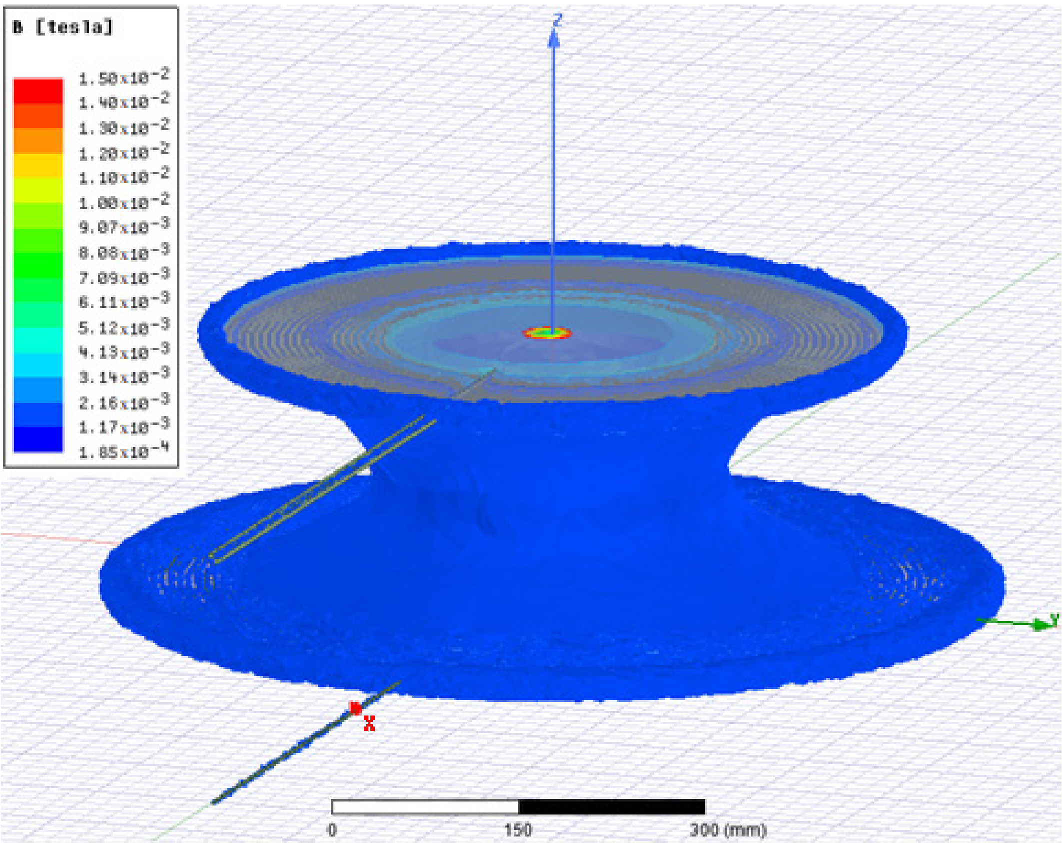

Figure 8. Magnetic field representation of the inductive coupling WPT system.

Table 7. Parameters of the system with increased k value.

a	Distance between coils	200 mm
Tft	Transmitter ferrite thickness	3 mm
Rft	Receiver ferrite thickness	1 mm
N_1	Number of turns of the transmitter coil	26 turns
N_2	Number of turns of the receiver coil	20 turns
$Rtin$	Transmitter coil inner radius	170 mm
$Rrin$	Receiver coil inner radius	130 mm
$Rtout$	Transmitter coil outer radius	352 mm
$Rrout$	Receiver coil outer radius	270 mm
dt	Pitch length of transmitter coil	7 mm
dr	Pitch length of receiver coil	7 mm
St	Transmitter coil cross section	2.5 mm^2
Sr	Receiver coil cross section	4 mm^2
k	Coupling coefficient	0.2671
L_1 (µH)	Inductance of transmitter coil	729.064
L_2 (µH)	Inductance of receiver coil	311.86
M (µH)	Mutual inductance	127.39
C_1 (nF)	Transmitter capacitor	86.94

Table 7. *Cont.*

C_2 (nF)	Receiver capacitor	203.26
Q_1	Transmitter quality factor	1.78
Q_2	Receiver quality factor	7.83
f_0	Resonant frequency	20 KHz
V_{source}	Input voltage (RMS)	200 V
R_L	Load	2.5, 5, 10 Ω

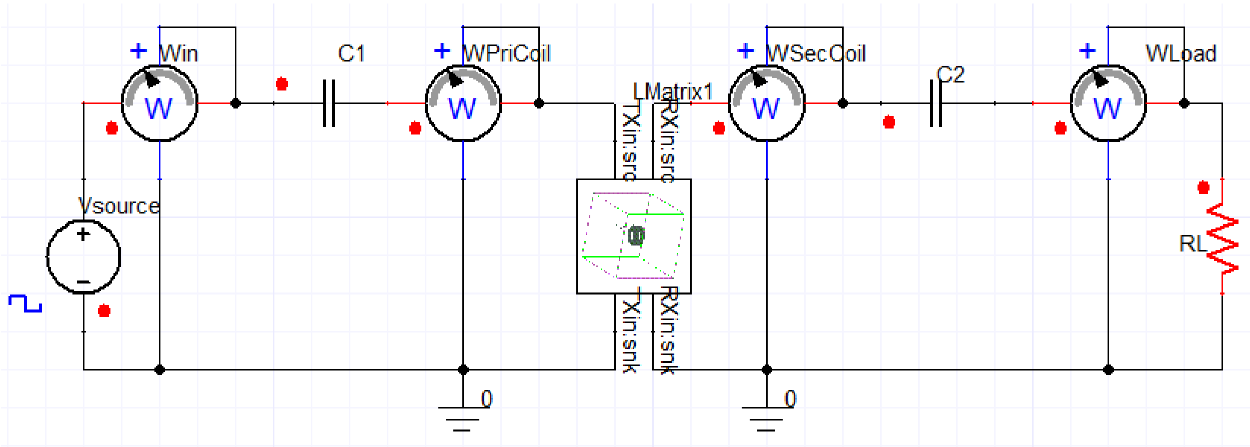

Figure 9. Simplorer circuit of the inductive coupling WPT system.

3. Simulation Results

When R_L = 2.5 Ω, the Simplorer efficiency graph of the inductive coupling WPT system is depicted in Figure 10, the voltage applied to the transmitter winding and the current flowing through the transmitter winding are shown in Figure 11, and the voltage between the ends of the load and the current flowing through the load are demonstrated in Figure 12.

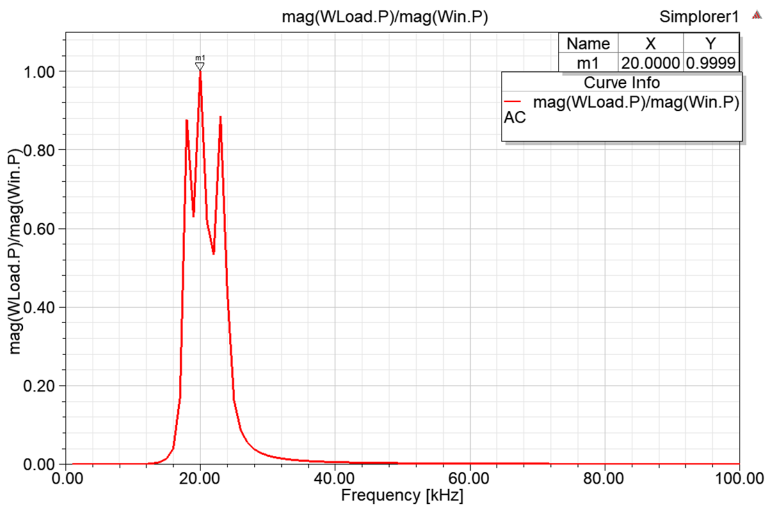

Figure 10. Simplorer efficiency graph of the inductive coupling WPT system (R_L = 2.5 Ω).

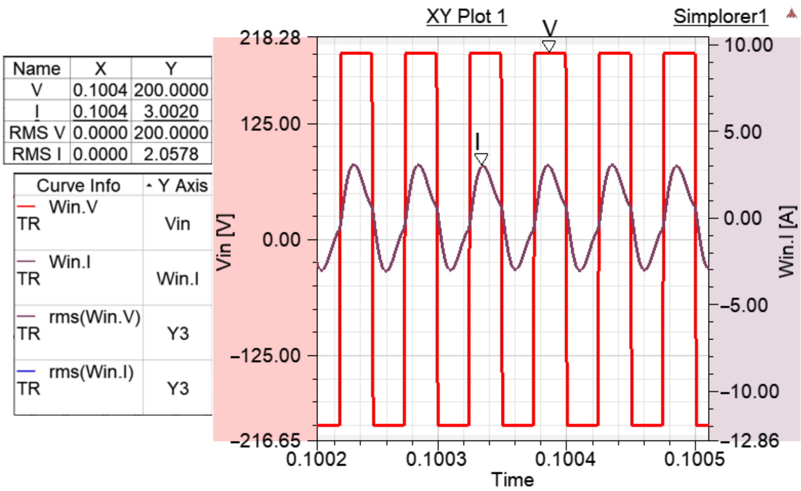

Figure 11. Voltage applied to the transmitter winding and current flowing through the transmitter winding (R_L = 2.5 Ω).

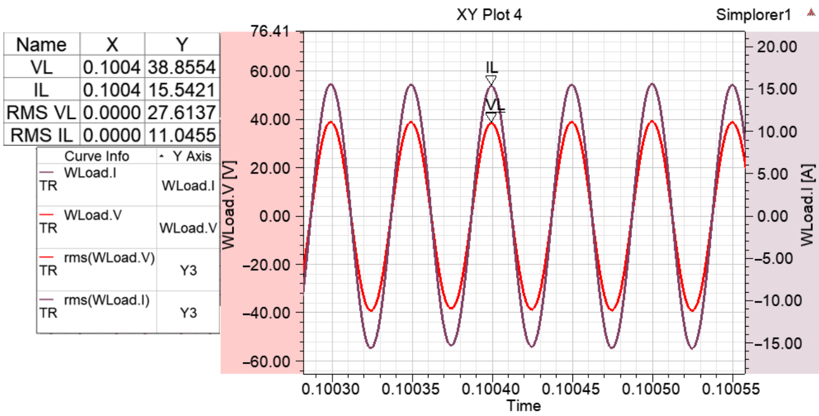

Figure 12. Voltage between the ends of the load and current flowing through the load (R_L = 2.5 Ω).

When R_L = 5 Ω, the Simplorer efficiency graph of the inductive coupling WPT system is shown in Figure 13, the voltage applied to the transmitter winding and the current flowing through the transmitter winding are depicted in Figure 14, and the voltage between the ends of the load and the current flowing through the load are illustrated in Figure 15.

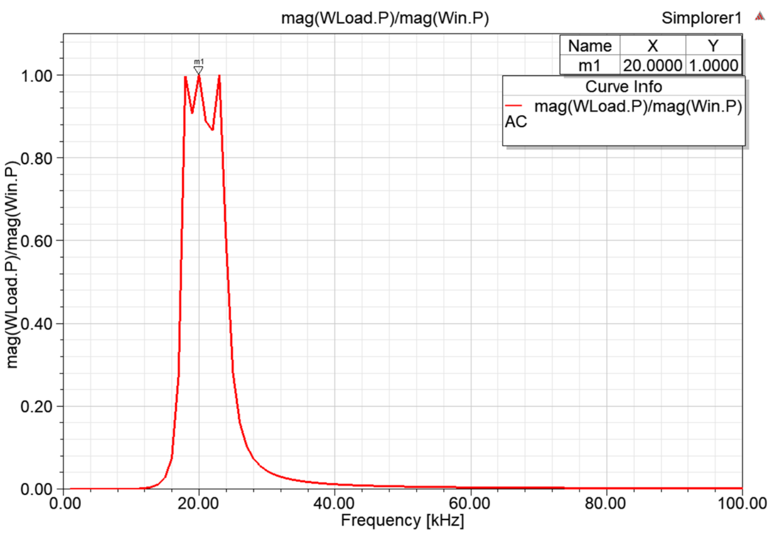

Figure 13. Simplorer efficiency graph of the inductive coupling WPT system (R_L = 5 Ω).

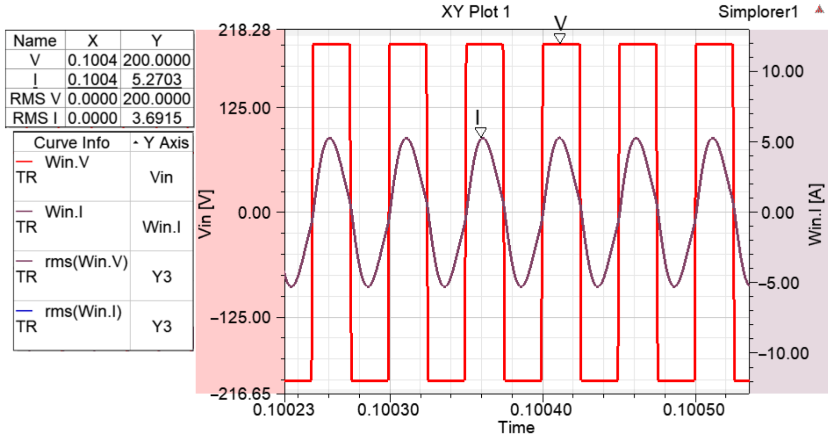

Figure 14. Voltage applied to the transmitter winding and current flowing through the transmitter winding (R_L = 5 Ω).

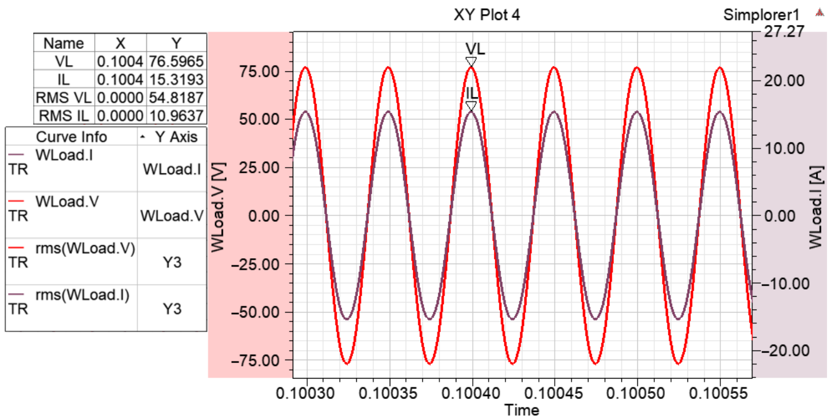

Figure 15. Voltage between the ends of the load and current flowing through the load (R_L = 5 Ω).

When R_L = 10 Ω, the Simplorer efficiency graph of the inductive coupling WPT system is shown in Figure 16, the voltage applied to the transmitter winding and the current flowing through the transmitter winding are illustrated in Figure 17, and the voltage between the ends of the load and the current flowing through the load are shown in Figure 18. The results obtained from the Maxwell model of the system are presented in Table 8. In addition, according to Equation (13), the power transferred to the load for each load value is calculated and is given in Table 8.

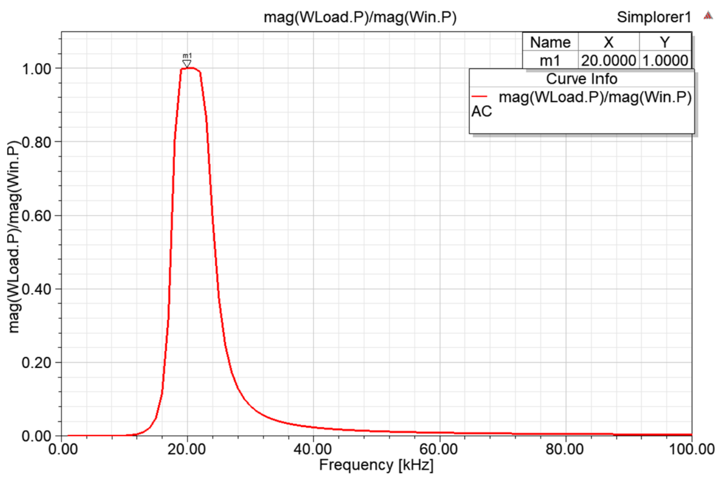

Figure 16. Simplorer efficiency graph of the inductive coupling WPT system (R_L = 10 Ω).

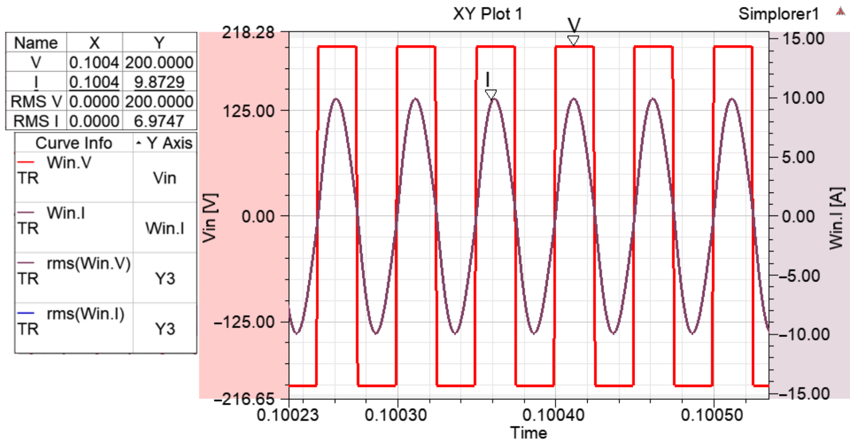

Figure 17. Voltage applied to the transmitter winding and current flowing through the transmitter winding (R_L = 10 Ω).

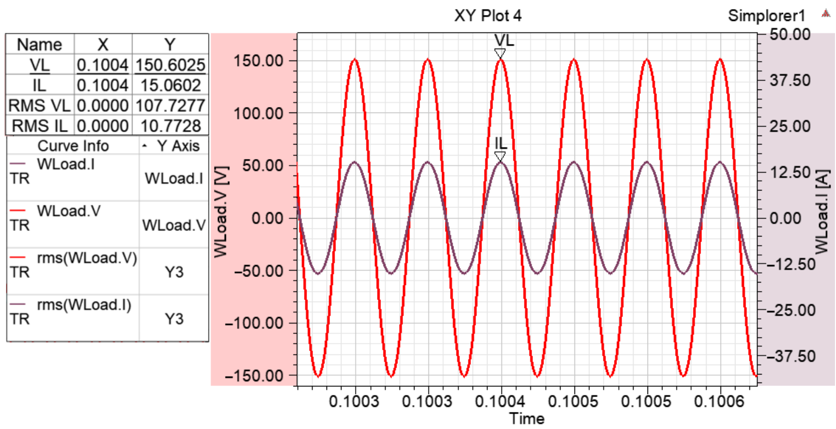

Figure 18. Voltage between the ends of the load and current flowing through the load (R_L = 10 Ω).

Table 8. Results obtained from the model.

	From the Model			According to Equation (13)		
	R_L			R_L		
	2.5 Ω	**5 Ω**	**10 Ω**	**2.5 Ω**	**5 Ω**	**10 Ω**
V_{in} (V)	200	200	200	200	200	200
I_1 (A)	2.0578	3.6915	6.9747	2.0578	3.6915	6.9747
P_{in} (W)	411.56	738.3	1394.94			
V_L (V)	27.6137	54.8187	107.7277			
I_L (A)	11.0455	10.9637	10.7728			
P_L (W)	305	601	1160.5	434.04	698.39	1246.56
η (%)	74.11	81.4	83.19			

4. Experimental Study

A prototype of the system with a high coupling coefficient was developed for experimental purposes. The transmitter winding comprises 26 turns of a 2.5 mm^2 conductor, while the receiver winding consists of 20 turns of a 4 mm^2 conductor. For the transmitter, four IXGN82N120C3H1 IGBTs are employed to switch 200 V DC. The maximum voltage and current ratings for this IGBT are 1200 Volts and 58 Amperes, respectively. A D_2 diode was used as a snubber to prevent damage to the IGBT during conduction and blocking [55].

Given the relatively low voltage between *G-E* and the relatively high voltage between *C-E*, the IGBTs should be isolated [56]. To achieve this, an IGBT driver, such as IR2113, is utilized. The circuit diagram of the inductive coupling WPT system is shown in Figure 19.

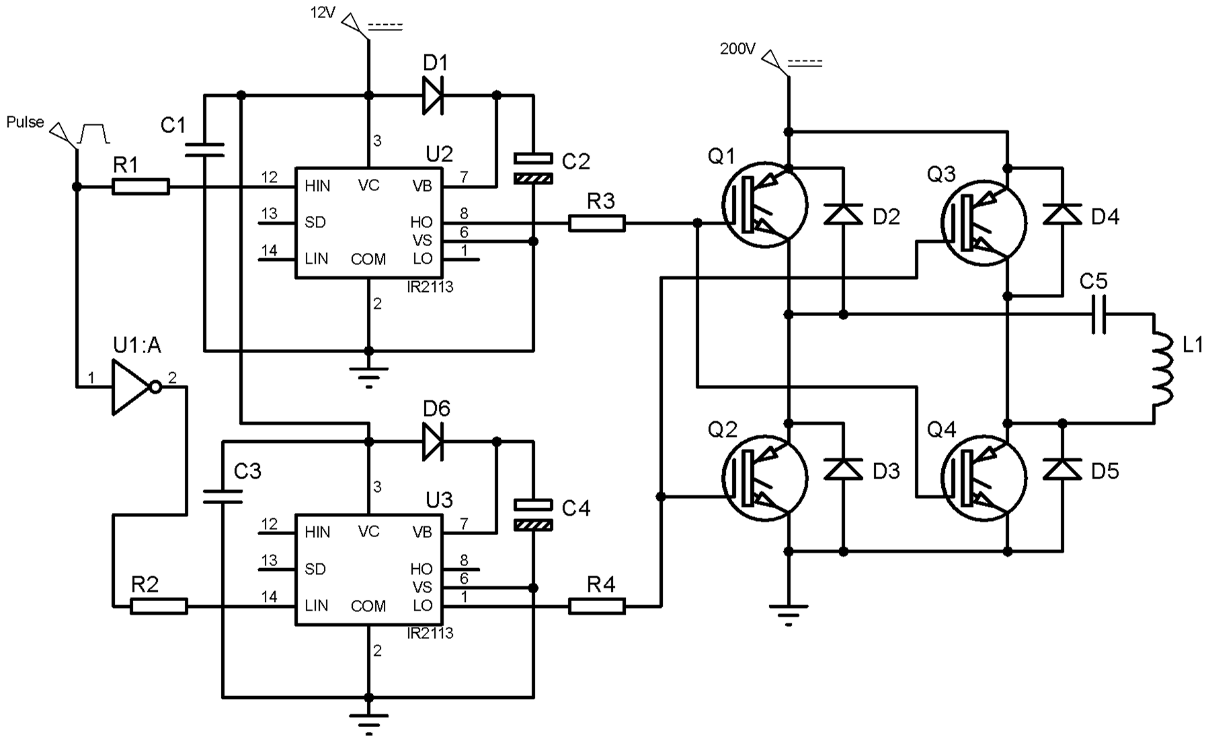

Figure 19. Circuit diagram of inductive coupling WPT system.

The image of the system prototype is shown in Figure 20. In Figure 21, capacitor C_1 was obtained by connecting 22 nF capacitors (C_1 = 86.9 nF). In Figure 22, capacitor C_2 was obtained by connecting 47 nF capacitors (C_2 = 203.66 nF).

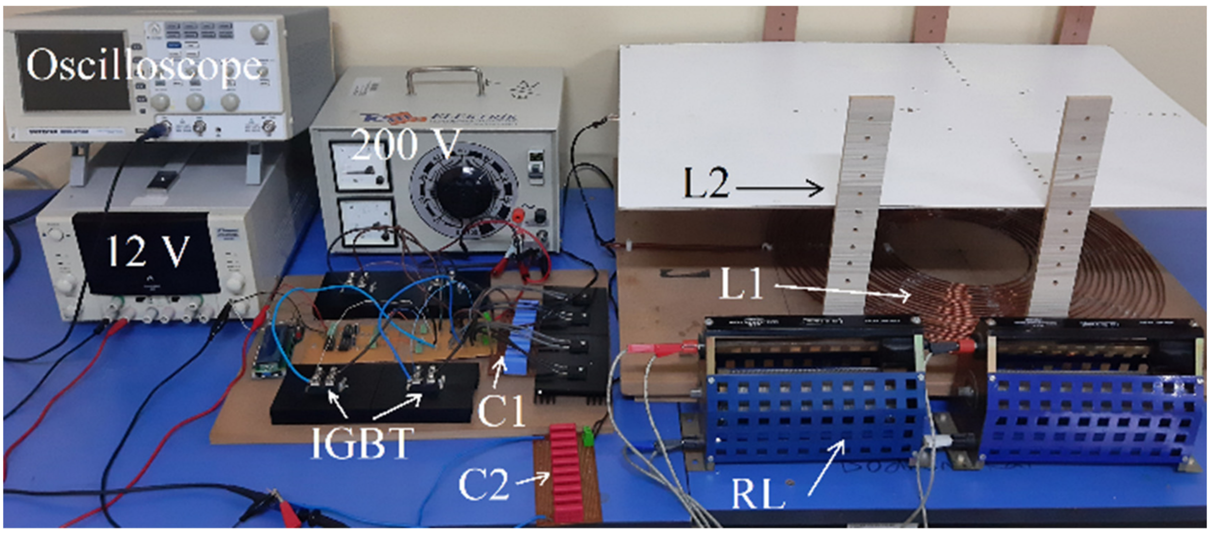

Figure 20. View of the system prototype.

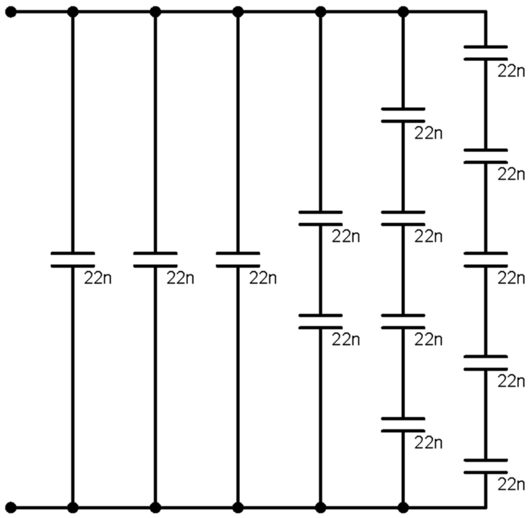

Figure 21. Obtaining capacitor C_1.

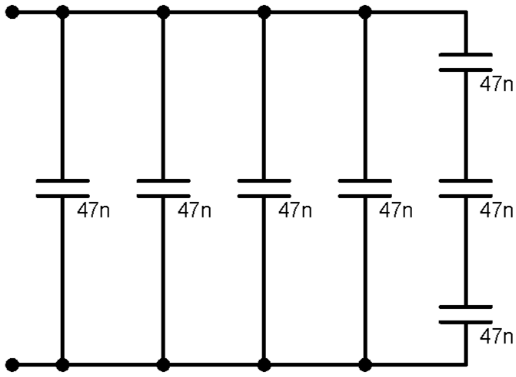

Figure 22. Obtaining capacitor C_2.

After the prototype of the system was implemented, the voltage applied to the transmitter winding and the voltage induced in the receiver winding were measured for R_L 2.5, 5, and 10 Ω, and the results obtained are given in Figures 23–26 and Table 9.

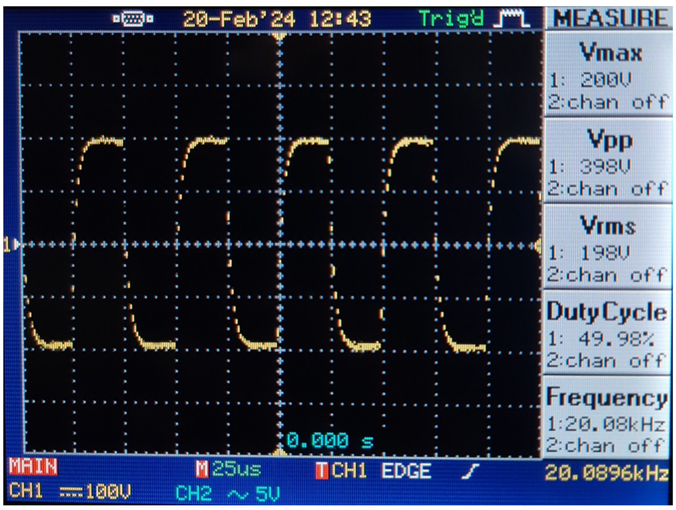

Figure 23. Voltage applied to the transmitter winding.

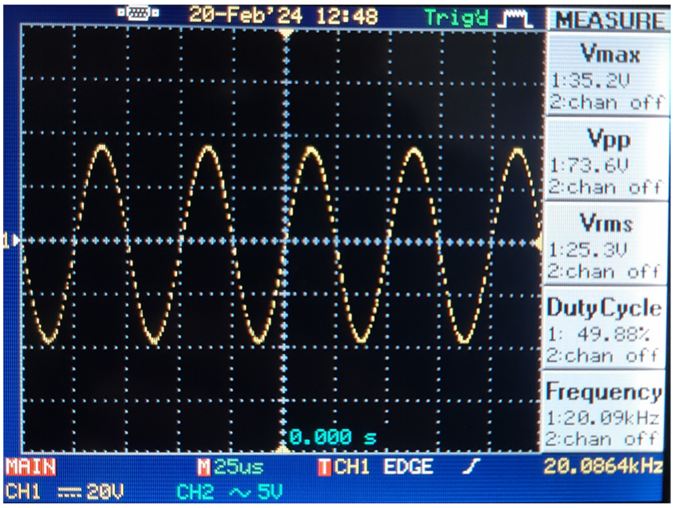

Figure 24. Voltage between the ends of the load (R_L = 2.5 Ω).

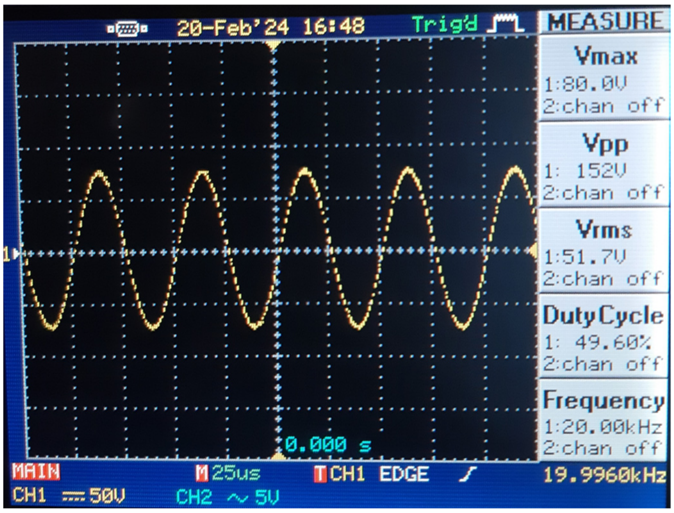

Figure 25. Voltage between the ends of the load (R_L = 5 Ω).

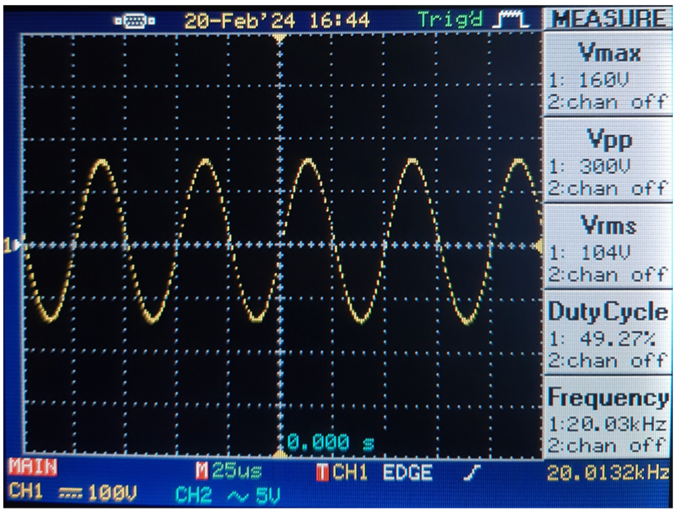

Figure 26. Voltage between the ends of the load (R_L = 10 Ω).

Table 9. Results from experimental studies.

	R_L		
	2.5 Ω	**5 Ω**	**10 Ω**
V_{in} (V)	200	200	200
I_1 (A)	1.95	3.47	6.76
P_{in} (W)	390	694	1352
V_L (V)	25.43	51.67	104.53
I_L (A)	10.28	9.71	9.68
P_L (W)	261.42	501.71	1011.85
η (%)	67.03	72.29	74.84

5. Results and Discussion

In this study, an inductive coupling WPT system with a notably higher coupling coefficient and consequently a higher efficiency was achieved. The first parameter is the coating of the outer surface of the coils with ferrite. The primary parameter considered was the application of the ferrite coating to the outer surface of the coils. A 3D Maxwell model of the system was employed to assess the impact of the ferrite coating on the coils' outer surfaces on the coupling coefficient. It was observed that when the ferrite thickness applied to the coils is 1 mm, there is a substantial increase in the k value. However, further increases in the ferrite thickness do not yield significant improvements in the k value. Consequently, a ferrite thickness (Rft) of 1 mm was chosen for the receiver coil, and a thickness (Tft) of 3 mm was selected for the transmitter coil, as elaborated in Section 2.1. In this configuration, the resulting k value was 0.2104, representing a notable increase of 29.47% from its initial value of 0.1625.

As the second parameter, the number of windings of the coils was investigated. Using the generated Maxwell model, we assessed the impact of altering the number of turns of the coils on the coupling coefficient. Specifically, the number of turns for the transmitter coil was set to 26, while the receiver coil was configured with 20 windings, as detailed in Section 2.2. In this configuration, the resulting k value was 0.1806, representing a notable increase of 11.13% from its initial value of 0.1625.

As the third parameter, variations in the inner and outer radii of the transmitter and receiver coils were investigated. By utilizing the Maxwell model of the system, we analyzed how changes in these dimensions affect the coupling coefficient. The outer radius of the transmitter coil was set to 320 mm, with an inner radius of 170 mm. Similarly, the outer radius of the receiver coil was established at 280 mm, while the inner radius was determined to be 130 mm, as detailed in Section 2.3. In this configuration, the resulting k value was 0.2012, reflecting a notable increase of 23.81% from its initial value of 0.1625.

As the final parameter, variations in the step distance between the windings were explored. The impact of altering the step distance on the coupling coefficient was assessed using a 3D Maxwell model. The highest k value was achieved when dt = 7 mm and dr = 7 mm, resulting in k = 0.1632. Consequently, there was an increase of 0.4% from its initial value of k = 0.1625.

At the conclusion of the investigation, a system with a heightened coupling coefficient was achieved, and both a 3D Maxwell model and Simplorer circuit for this system were developed. Utilizing these models, the voltage applied to the transmitter winding, the current flowing through the transmitter winding, the voltage at the load ends, and the current flowing through the load were determined for load resistances of 2.5, 5, and 10 Ω. From these values, the input and output power of the system were calculated, allowing for the determination of system efficiency.

Subsequently, a prototype of the system with a high coupling coefficient was constructed. The outcomes from experimental studies were compared with those obtained from the model, and the results are presented comparatively in Figures 27–29. As illustrated in Figure 27, both the model and experimental study demonstrate an increase in input power as the load resistance increases. Similarly, Figure 28 indicates that as the load resistance increases, the output power rises in both the model and experimental study. Moreover, as depicted in Figure 29, the efficiency of the system also increases with the rise in load resistance, observed in both the model and experimental study.

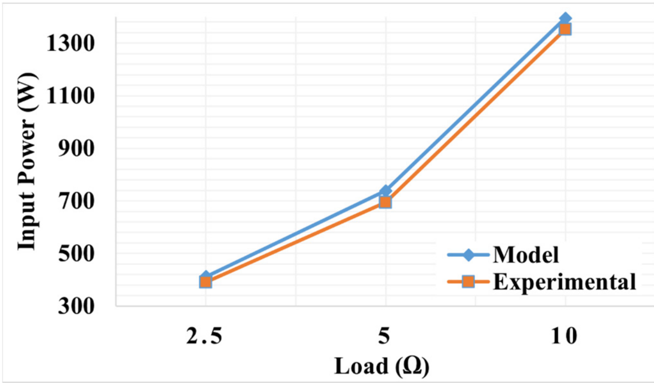

Figure 27. Comparison of input powers according to load.

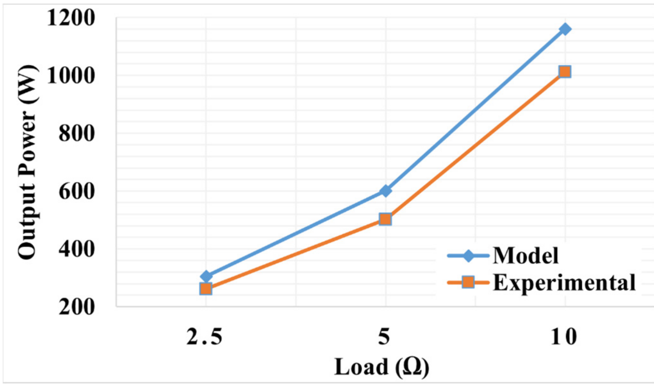

Figure 28. Comparison of output powers according to load.

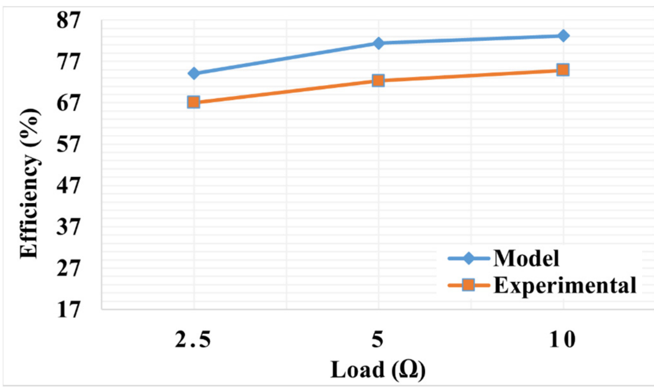

Figure 29. Comparison of efficiencies according to load.

6. Conclusions

In this study, an inductive coupling WPT system from previous research was revised with the objective of enhancing its coupling coefficient and efficiency. To achieve this goal, the impact of four system parameters (the ferrite coating of the coils, number of windings of the coils, radius of the coils, and distance between the windings of the coils) on the coupling coefficient was investigated. To analyze the effect of each parameter on the coupling coefficient, a 3D Maxwell model of the system was constructed. Each parameter was individually modified while keeping the others constant in the Maxwell model to isolate its impact.

Subsequently, a system with an improved coupling coefficient was achieved through this investigation. Consequently, a 3D Maxwell model and a Maxwell Simplorer circuit model of the system with the enhanced coupling coefficient were developed. Within the Simplorer circuit model, the input and output values of the system were investigated for load resistances of 2.5, 5, and 10 Ω.

Ultimately, a prototype of the system with an enhanced coupling coefficient was successfully constructed, and the input and output values were measured accordingly. The prototype developed is characterized not only by its cost effectiveness and simplicity but also by its level of efficiency.

Upon the conclusion of our studies, the results derived from our experimental investigations were compared with those obtained from the model. It became evident that the outcomes obtained from the experimental studies were slightly lower. This disparity can be attributed to factors such as coupling and other inherent losses within the system.

One of the important parameters in the inductive WPT system is the coupling coefficient, as it significantly influences system efficiency. A higher coupling coefficient corresponds to increased system efficiency. The significance of this study lies in its clarification of how specific parameters impact the coupling coefficient. In the previous study, the coupling coefficient was 0.1625, with an efficiency of 78.3. Through modifications to four parameters, the coupling coefficient was increased to 0.2671, concurrently raising the efficiency to 81.4. The correct selection of system parameters holds the potential to enhance system efficiency. Although the efficiency observed in this study appears to be slightly low, further research efforts will focus on parameters aimed at augmenting efficiency. This investigation will be extended to explore the impact of coil shape, operating frequency, and compensation topology on system efficiency.

In future studies, the issue of misalignment will be explored, which could significantly affect the performance of the system. Additionally, methods to detect and mitigate the impact of foreign substances that may enter the coils will be studied.

Funding: This research received no external funding.

Data Availability Statement: The original contributions presented in the study are included in the article, further inquiries can be directed to the corresponding author.

Conflicts of Interest: The author declares no conflicts of interest.

References

1. Kalwar, K.A.; Aamir, M.; Mekhilef, S. Inductively Coupled Power Transfer (ICPT) for Electric Vehicle Charging—A Review. *Renew. Sustain. Energy Rev.* **2015**, *47*, 462–475. [CrossRef]
2. Pedder, D.A.G.; Brown, A.D.; Skinner, J.A. A Contactless Electrical Energy Transmission System. *IEEE Trans. Ind. Electron.* **1999**, *46*, 23–30. [CrossRef]
3. Aditya, K.; Williamson, S.S. Design Considerations for Loosely Coupled Inductive Power Transfer (IPT) System for Electric Vehicle Battery Charging-A Comprehensive Review. In Proceedings of the 2014 IEEE Transportation Electrification Conference and Expo (ITEC), Dearborn, MI, USA, 15–18 June 2014. [CrossRef]
4. Wu, H.H.; Gilchrist, A.; Sealy, K.D.; Bronson, D. A High Efficiency 5 KW Inductive Charger for EVs Using Dual Side Control. *IEEE Trans. Ind. Inform.* **2012**, *8*, 585–595. [CrossRef]
5. Green, A.W.; Boys, J.T. 10 KHz Inductively Coupled Power Transfer-Concept and Control. In Proceedings of the 1994 Fifth International Conference on Power Electronics and Variable-Speed Drives, London, UK, 26–28 October 1994. [CrossRef]
6. Covic, G.A.; Boys, J.T. Inductive Power Transfer. *Proc. IEEE* **2013**, *101*, 1276–1289. [CrossRef]
7. Diekhans, T.; De Doncker, R.W. A Dual-Side Controlled Inductive Power Transfer System Optimized for Large Coupling Factor Variations and Partial Load. *IEEE Trans. Power Electron.* **2015**, *30*, 6320–6328. [CrossRef]
8. Sun, K.; Niu, W. SPWM Inverter Control for Wireless Constant Current and Voltage Charging. *World Electr. Veh. J.* **2023**, *14*, 111. [CrossRef]
9. Kan, T.; Nguyen, T.D.; White, J.C.; Malhan, R.K.; Mi, C.C. A New Integration Method for an Electric Vehicle Wireless Charging System Using LCC Compensation Topology: Analysis and Design. *IEEE Trans. Power Electron.* **2017**, *32*, 1638–1650. [CrossRef]

10. Gbey, E.; Turkson, R.F.; Lee, S. A Bibliometric Survey of Research Output on Wireless Charging for Electric Vehicles. *World Electr. Veh. J.* **2022**, *13*, 37. [CrossRef]
11. Takanashi, H.; Sato, Y.; Kaneko, Y.; Abe, S.; Yasuda, T. A Large Air Gap 3 KW Wireless Power Transfer System for Electric Vehicles. In Proceedings of the 2012 IEEE Energy Conversion Congress and Exposition (ECCE), Raleigh, NC, USA, 15–20 September 2012. [CrossRef]
12. Chen, R.; Zheng, C.; Zahid, Z.U.; Faraci, E.; Yu, W.; Lai, J.S.; Senesky, M.; Anderson, D.; Lisi, G. Analysis and Parameters Optimization of a Contactless IPT System for EV Charger. In Proceedings of the 2014 IEEE Applied Power Electronics Conference and Exposition-APEC 2014, Fort Worth, TX, USA, 16–20 March 2014. [CrossRef]
13. Keeling, N.A.; Covic, G.A.; Boys, J.T. A Unity-Power-Factor IPT Pickup for High-Power Applications. *IEEE Trans. Ind. Electron.* **2010**, *57*, 744–751. [CrossRef]
14. Yilmaz, M.; Krein, P.T. Review of Battery Charger Topologies, Charging Power Levels, and Infrastructure for Plug-In Electric and Hybrid Vehicles. *IEEE Trans. Power Electron.* **2013**, *28*, 2151–2169. [CrossRef]
15. Qiu, C.; Chau, K.T.; Liu, C.; Chan, C.C. Overview of Wireless Power Transfer for Electric Vehicle Charging. In Proceedings of the 2013 International Battery, Hybrid and Fuel Cell Electric Vehicle Symposium (EVS27), Barcelona, Spain, 17–20 November 2013. [CrossRef]
16. Zhao, J.; Cai, T.; Duan, S.; Feng, H.; Chen, C.; Zhang, X. A General Design Method of Primary Compensation Network for Dynamic WPT System Maintaining Stable Transmission Power. *IEEE Trans. Power Electron.* **2016**, *31*, 8343–8358. [CrossRef]
17. Bi, Z.; Kan, T.; Mi, C.C.; Zhang, Y.; Zhao, Z.; Keoleian, G.A. A Review of Wireless Power Transfer for Electric Vehicles: Prospects to Enhance Sustainable Mobility. *App. Energy* **2016**, *179*, 413–425. [CrossRef]
18. Tan, L.; Pan, S.; Huang, X.; Xu, C. System Optimization for Wireless Power Transfer System with Double Transmitters. In Proceedings of the 2017 IEEE PELS Workshop on Emerging Technologies: Wireless Power Transfer (WoW), Chongqing, China, 20–22 May 2017. [CrossRef]
19. Madawala, U.K.; Thrimawithana, D.J. A Bidirectional Inductive Power Interface for Electric Vehicles in V2G Systems. *IEEE Trans. Ind. Electron.* **2011**, *58*, 4789–4796. [CrossRef]
20. Lin, F.Y.; Zaheer, A.; Budhia, M.; Covic, G.A. Reducing Leakage Flux in IPT Systems by Modifying Pad Ferrite Structures. In Proceedings of the 2014 IEEE Energy Conversion Congress and Exposition (ECCE), Pittsburgh, PA, USA, 14–18 September 2014. [CrossRef]
21. Zhang, P.; Yang, Q.; Zhang, X.; Li, Y.; Li, Y. Comparative Study of Metal Obstacle Variations in Disturbing Wireless Power Transmission System. *IEEE Trans. Magn.* **2017**, *53*, 1–4. [CrossRef]
22. Zhang, X.; Ni, X.; Yang, Q.; Wei, B.; Wang, S. Analysis of Electromagnetic Force on Metal Objects in Vertical Direction of Wireless Power Transfer. In Proceedings of the 2019 IEEE PELS Workshop on Emerging Technologies: Wireless Power Transfer (WoW), London, UK, 18–21 June 2019. [CrossRef]
23. Bekiroglu, N.; Agcal, A.; Ozcira, S. Validation of Wireless Power Transfer by Using 3d Representation of Magnetically Coupled Resonators Considering Peak Efficiency. *J. Magn.* **2018**, *23*, 11–17. [CrossRef]
24. Lee, S.; Jung, G.; Shin, S.; Kim, Y.; Song, B.; Shin, J.; Cho, D. The Optimal Design of High-Powered Power Supply Modules for Wireless Power Transferred Train. In Proceedings of the 2012 Electrical Systems for Aircraft, Railway and Ship Propulsion, Bologna, Italy, 16–18 October 2012. [CrossRef]
25. Agcal, A.; Bekiroglu, N.; Ozcira, S. Comparison of Magnetic Resonant Coupling Wireless Power Transfer Systems within Aligned and Unaligned Positions and Determining Their Limits. *J. Magn.* **2016**, *21*, 652–659. [CrossRef]
26. Aditya, K. Design and Characteristics of Series–Series and Series–Parallel Topologies Fed from Constant-Voltage Fixed-Frequency Supply. *Sādhanā* **2017**, *42*, 163–171. [CrossRef]
27. Budhia, M.; Boys, J.T.; Covic, G.A.; Huang, C.Y. Development of a Single-Sided Flux Magnetic Coupler for Electric Vehicle IPT Charging Systems. *IEEE Trans. Ind. Electron.* **2013**, *60*, 318–328. [CrossRef]
28. Hentschel, U.; Helwig, M.; Winkler, A.; Modler, N. Simulation of Foreign Object Detection Using Passive Inductive Sensors in a Wireless Charging System for Electric Vehicles. *World Electr. Veh. J.* **2023**, *14*, 241. [CrossRef]
29. Liu, C.; Jiang, C.; Qiu, C. Overview of Coil Designs for Wireless Charging of Electric Vehicle. In Proceedings of the 2017 IEEE PELS Workshop on Emerging Technologies: Wireless Power Transfer (WoW), Chongqing, China, 20–22 May 2017. [CrossRef]
30. Sallán, J.; Villa, J.L.; Llombart, A.; Sanz, J.F. Optimal Design of ICPT Systems Applied to Electric Vehicle Battery Charge. *IEEE Trans. Ind. Electron.* **2009**, *56*, 2140–2149. [CrossRef]
31. Triviño-Cabrera, A.; González-González, J.M.; Aguado, J.A. *Wireless Power Transfer for Electric Vehicles: Foundations and Design Approach*, 1st ed.; Springer: Cham, Switzerland, 2020; pp. 6–74. [CrossRef]
32. Stielau, O.H.; Covic, G.A. Design of Loosely Coupled Inductive Power Transfer Systems. In Proceedings of the 2000 International Conference on Power System Technology. Proceedings, Perth, WA, Australia, 4–7 December 2000. [CrossRef]
33. Mahesh, A.; Chokkalingam, B.; Mihet-Popa, L. Inductive Wireless Power Transfer Charging for Electric Vehicles–A Review. *IEEE Access* **2021**, *9*, 137667–137713. [CrossRef]
34. Chopra, S.; Bauer, P. Analysis and Design Considerations for a Contactless Power Transfer System. In Proceedings of the 2011 IEEE 33rd International Telecommunications Energy Conference (INTELEC), Amsterdam, The Netherlands, 9–13 October 2011. [CrossRef]
35. García, X.D.T.; Vázquez, J.; Roncero-Sánchez, P. Design, Implementation Issues and Performance of an Inductive Power Transfer System for Electric Vehicle Chargers with Series–Series Compensation. *IET Power Electron.* **2015**, *8*, 1920–1930. [CrossRef]

36. Wang, C.S.; Stielau, O.H.; Covic, G.A. Design Considerations for a Contactless Electric Vehicle Battery Charger. *IEEE Trans. Ind. Electron.* **2005**, *52*, 1308–1314. [CrossRef]
37. Villa, J.L.; Sallan, J.; Osorio, J.F.S.; Llombart, A. High-Misalignment Tolerant Compensation Topology for ICPT Systems. *IEEE Trans. Ind. Electron.* **2012**, *59*, 945–951. [CrossRef]
38. Wang, C.S.; Covic, G.A.; Stielau, O.H. Power Transfer Capability and Bifurcation Phenomena of Loosely Coupled Inductive Power Transfer Systems. *IEEE Trans. Ind. Electron.* **2004**, *51*, 148–157. [CrossRef]
39. Bouanou, T.; El Fadil, H.; Lassioui, A.; Bentalhik, I.; Koundi, M.; El Jeilani, S. Design Methodology and Circuit Analysis of Wireless Power Transfer Systems Applied to Electric Vehicles Wireless Chargers. *World Electr. Veh. J.* **2023**, *14*, 117. [CrossRef]
40. Zhang, Y.; Shen, Z.; Wu, Y.; Wang, H.; Pan, W. Dual-Side Phase-Shift Control for Strongly Coupled Series–Series Compensated Electric Vehicle Wireless Charging Systems. *World Electr. Veh. J.* **2022**, *13*, 6. [CrossRef]
41. Bentalhik, I.; Lassioui, A.; EL Fadil, H.; Bouanou, T.; Rachid, A.; EL Idrissi, Z.; Hamed, A.M. Analysis, Design and Realization of a Wireless Power Transfer Charger for Electric Vehicles: Theoretical Approach and Experimental Results. *World Electr. Veh. J.* **2022**, *13*, 121. [CrossRef]
42. Tan, P.; Peng, T.; Gao, X.; Zhang, B. Flexible Combination and Switching Control for Robust Wireless Power Transfer System with Hexagonal Array Coil. *IEEE Trans. Power Electron.* **2021**, *36*, 3868–3882. [CrossRef]
43. Ramezani, A.; Narimani, M. Optimized Electric Vehicle Wireless Chargers with Reduced Output Voltage Sensitivity to Misalignment. *IEEE J. Emerg. Sel. Top. Power Electron.* **2019**, *8*, 3569–3581. [CrossRef]
44. Zhou, J.; Yao, P.; Guo, K.; Cao, P.; Zhang, Y.; Ma, H. A Heterogeneous Inductive Power Transfer System for Electric Vehicles with Spontaneous Constant Current and Constant Voltage Output Features. *Electronics* **2020**, *9*, 1978. [CrossRef]
45. Foote, A.; Costinett, D.; Kusch, R.; Mohammad, M.; Onar, O. Fourier Analysis and Loss Modeling for Inductive Wireless Electric Vehicle Charging with Reduced Stray Field. *IEEE Trans. Transp. Electrif.* **2024**. [CrossRef]
46. Scientific Applications International Corporation. Life Cycle Assessment: Principles and Practice. National Risk Management Research Laboratory Office of Research and Development, U.S. Environmental Protection Agency. 2006. Available online: https://nepis.epa.gov/Exe/ZyPDF.cgi/P1000L86.PDF?Dockey=P1000L86.PDF (accessed on 5 March 2024).
47. Bi, Z.; De Kleine, R.; Keoleian, G.A. Integrated Life Cycle Assessment and Life Cycle Cost Model for Comparing Plug-in versus Wireless Charging for an Electric Bus System. *J. Ind. Ecol.* **2016**, *21*, 344–355. [CrossRef]
48. Obayashi, S.; Tsukahara, H. EMC issues on wireless power transfer. In Proceedings of the 2014 International Symposium on Electromagnetic Compatibility, Tokyo, Japan, 12–16 May 2014.
49. Zimmer, S.; Helwig, M.; Lucas, P.; Winkler, A.; Modler, N. Investigation of Thermal Effects in Different Lightweight Constructions for Vehicular Wireless Power Transfer Modules. *World Electr. Veh. J.* **2020**, *11*, 67. [CrossRef]
50. Lin, J.C. Safety of Wireless Power Transfer. *IEEE Access* **2021**, *9*, 125342–125347. [CrossRef]
51. Kim, D.; Kim, H.; Huang, A.; He, Q.; Zhang, H.; Ahn, S.; Zhu, Y.; Fan, J. Analysis and Introduction of Effective Permeability with Additional Air-gaps on Wireless Power Transfer Coils for Electric Vehicle Based on SAE J2954 Recommended Practice. *Energies* **2019**, *12*, 4797. [CrossRef]
52. International Electrotechnical Commission. IEC 61980-1 EV WPT Systems. Available online: https://webstore.iec.ch/preview/info_iec61980-1%7Bed1.0%7Den.pdf (accessed on 5 March 2024).
53. *ISO 19363:2020*; Electrically Propelled Road Vehicles, Magnetic Field Wireless Power Transfer, Safety and Interoperability Requirements. International Organization for Standardization: Geneva, Switzerland, 2020. Available online: https://www.iso.org/standard/73547.html (accessed on 5 March 2024).
54. Sari, V. Design and Model of an Inductive Wireless Power Transfer System for Electric Vehicles. In Proceedings of the 4th International Congress on Natural and Applied Sciences, Rio de Janeiro, Brazil, 13–15 March 2023; Available online: https://www.iksadameica.org/_files/ugd/614b1f_f7b977c28570493dbd00b60ed7be97da.pdf (accessed on 5 March 2024).
55. ON Semiconductor Corporation, Application Note 9020, IGBT Basic II. Available online: https://www.onsemi.com/pub/collateral/an-9020.pdf (accessed on 22 January 2024).
56. Infineon Technologies, IR2113 High and Low Side Driver Datasheet. Available online: https://www.infineon.com/dgdl/Infineon-IR2110-DataSheet-v01_00-EN.pdf?fileId=5546d462533600a4015355c80333167e (accessed on 22 January 2024).